

# FakeScope: Large Multimodal Expert Model for Transparent AI-Generated Image Forensics

Yixuan Li, Yu Tian, Yipo Huang, Wei Lu, *Member, IEEE*, Shiqi Wang<sup>†</sup>, *Senior Member, IEEE*, Weisi Lin, *Fellow, IEEE* and Anderson Rocha, *Fellow, IEEE*

**Abstract**—The rapid and unrestrained advancement of generative artificial intelligence (AI) presents a double-edged sword: while enabling unprecedented creativity, it also facilitates the generation of highly convincing deceptive content, undermining societal trust. As image generation techniques become increasingly sophisticated, detecting synthetic images is no longer just a binary task—it necessitates interpretable, context-aware methodologies that enhance trustworthiness and transparency. However, existing detection models primarily focus on classification, offering limited explanatory insights into image authenticity. In this work, we propose FakeScope, an expert multimodal model (LMM) tailored for AI-generated image forensics, which not only identifies AI-synthetic images with high accuracy but also provides rich, interpretable, and query-driven forensic insights. To this end, we first construct FakeChain dataset that contains linguistic authenticity reasoning based on visual trace evidence, developed through a novel human-machine collaborative framework. Building upon it, we further present FakeInstruct, the largest multimodal instruction tuning dataset containing 2 million visual instructions tailored to enhance forensic awareness in LMMs. Leveraging the knowledge of FakeInstruct, FakeScope achieves state-of-the-art performance in both closed-ended and open-ended forensic scenarios. It can distinguish synthetic images with high accuracy while offering coherent and insightful explanations, free-form discussions on fine-grained forgery attributes, and actionable enhancement strategies. Notably, despite being trained exclusively on qualitative hard labels, FakeScope demonstrates remarkable zero-shot quantitative capability on detection, enabled by our proposed token-based probability estimation strategy. Furthermore, FakeScope exhibits strong generalization and in-the-wild ability, ensuring its applicability in real-world scenarios. The data, model, and demo will be publicly released on <https://github.com/Yixuan423/FakeScope>.

**Index Terms**—AI-generated image detection, large multimodal models, forensic investigation, trustworthiness.

## I. INTRODUCTION

With the rapid development of image generation techniques, AI-synthesized images are becoming increasingly indistinguishable from genuine ones [1], [2]. While this prosperity has driven innovation, it also introduces significant

Y. Li, Y. Tian and S. Wang are with the College of Computing, City University of Hong Kong, Hong Kong SAR (e-mail: yixuanli423@gmail.com; ytian73-c@my.cityu.edu.hk; shiqi.wang@cityu.edu.hk).

W. Lu is with the School of Computer Science and Engineering, Ministry of Education Key Laboratory of Information Technology, Guangdong Province Key Laboratory of Information Security Technology, Sun Yat-Sen University, Guangzhou 510006, China (e-mail: luwei3@mail.sysu.edu.cn).

Y. Huang and W. Lin are with the College of Computing and Data Science, Nanyang Technological University, Singapore (e-mail: yipo.huang@ntu.edu.sg, wslin@ntu.edu.sg).

A. Rocha is with the Artificial Intelligence Lab. (Recod.ai) at the University of Campinas, Campinas 13084-851, Brazil (e-mail: arrocha@unicamp.br)

<sup>†</sup>Corresponding author: Shiqi Wang.

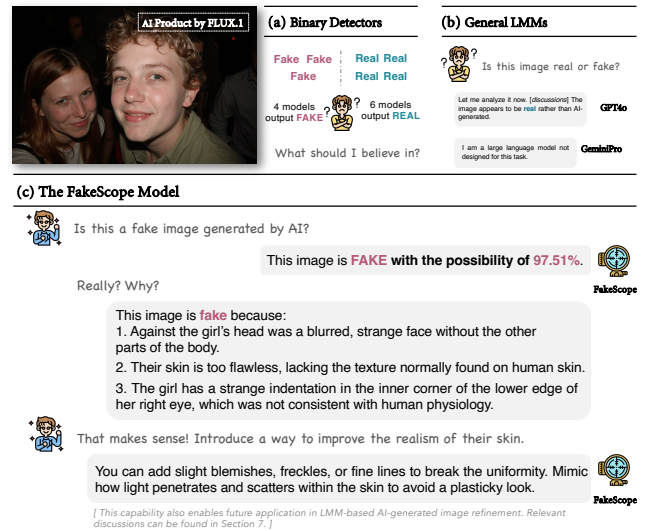


Fig. 1. Comparative illustration of image forensic model evolution. (a) Binary detectors; (b) general LMMs; and (c) FakeScope, which translates visual abnormalities into human-understandable cues—much like trace evidence in forensics—using natural language.

cybersecurity threats, including misinformation, propaganda, and fraud. In response, substantial efforts have been made to detect AI-generated content in recent years [3]–[6]. However, as generative models continue to evolve, concerns over the reliability and trustworthiness of detection systems in real-world applications persist. Addressing these challenges requires enhancing the transparency of AI-generated image detection models. We advocate for a paradigm shift in which image synthesis detection goes beyond binary classification, incorporating explainability to provide contextual insights into authenticity assisting trustworthiness.

Until recently, AI-generated image detection was predominantly framed as a binary classification task. Conventional approaches rely on unimodal architectures such as convolutional neural networks (CNNs) and vision transformers (ViTs) to classify images as either real or synthetic, significantly aiding in mitigating the spread of synthetic content. However, these early methods largely overlooked the need for transparency, offering little more than abstract heatmaps derived from deep neural network features as visual explanations. Recent research has shown that AI-generated images increasingly pass sanity checks by humans and machines [1], [7], leading to human-machine or machine-machine disagreements. As illustrated in Fig. 1 (a), different detectors can yield inconsistent decisions,

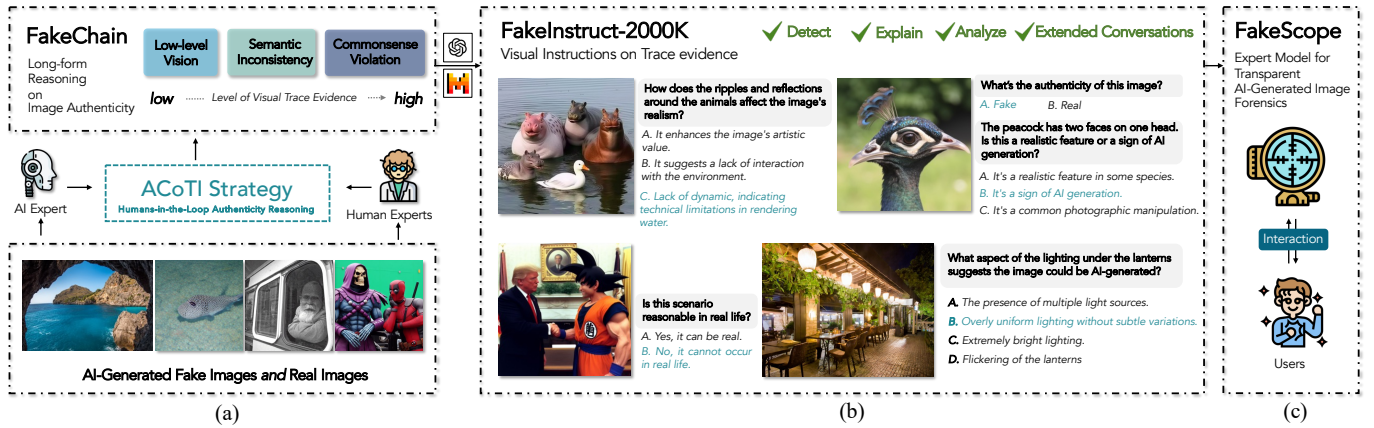


Fig. 2. Contributions of this work. (a) FakeChain dataset, containing reasoning on image authenticity, constructed via the proposed *ACoTI* strategy (Sec. III); (b) FakeInstruct dataset, containing 2 million visual instructions of image forensic knowledge (Sec. IV); (c) FakeScope model, the expert model for transparent AI-generated image forensics, capable of multi-dimensional forensic capabilities (Sec. V).

significantly reducing practical utility. In contrast, in Fig.1(c), a transparent model can provide additional insights via visual trace evidence to enhance interpretability. **Therefore, we anticipate more trustworthy paradigms that exceed binary detectors for achieving transparent forensics of AI-generated images.** Such a model would enable human oversight, mitigate detection biases, and foster better confidence in AI-generated content forensics [2].

With the advent of multimodal models, visual-language approaches have started to emerge. Zhang *et al.* [8] introduced textual template descriptions to improve explainable deepfake face detection. Sun *et al.* [9] formulated brief descriptions by integrating forgery regions and candidate types using a predefined template. Li *et al.* [7] and Ye *et al.* [10] explored the capabilities of large multimodal models (LMMs) in the forensic analysis of AI-generated images. In [11]–[13], LMMs are incorporated to localize tampering forgeries and exhibits substantial effectiveness. Besides, LMMs are employed to assist in improving detection accuracy. In [14] and [15], conventional detectors are combined with LMMs to improve detection accuracy. Wen *et al.* [16] train a binary classifier with ViT intermediate features and use LMMs to explain the detection. These studies establish a concrete foundation for the transition from unimodal to multimodal approaches in the area of AI-generated image forensics. Nevertheless, due to the inherent limitations of LMMs as classifiers [17], previous approaches have struggled to balance detection accuracy and transparency, often relying on separate strategies and training procedures to fulfill multi-dimensional forensic tasks. **Therefore, there is an urgent need for a unified forensic expert model for AI-generated images capable of multiple forensic tasks in diversified scenarios.**

Inspired by the above insights, we present **FakeScope**, a unified expert model for *transparent* and *versatile* AI-generated image forensics. It leverages the remarkable cross-modality ability of generally pretrained LMMs while being systematically enhanced for universal forensic awareness. Specifically, it is designed with three key objectives: (1)

comprehension on trace evidence and authenticity; (2) faithful response to diverse user queries; and (3) qualitative and quantitative detection without model extension. To achieve these, we collect and leverage forensic knowledge to improve LMMs' forensic awareness on AI-generated images. As shown in Fig. 2(a), we first construct **FakeChain**, a large-scale multimodal dataset containing long and comprehensive reasoning on image authenticity as forensic knowledge source, developed via a cost-efficient human-in-the-loop strategy. We further enrich FakeChain to create **FakeInstruct**, a gigantic-scale dataset comprising **2 million** visual instructions to enhance diverse forensic abilities of LMMs (Fig. 2(b)). Extensive experiments demonstrate that FakeInstruct consistently improves the forensic capabilities of general LMMs, and the proposed **FakeScope** (Fig. 2(c)) exhibits state-of-the-art (SOTA) performance in detecting, explaining, analyzing, and discussing AI-generated images. In particular, it can generalize well to unseen image content, generation models, and even user-created contents. Our core contributions are as follows.

- We present **FakeChain**, a large-scale multimodal dataset with coherent reasoning flow from visual trace evidence to image authenticity. It is collected through our proposed *Anthropomorphic Chain-of-Thought Inference (ACoTI)* scheme, a cost-effective human-machine collaboration strategy that requires minimal human annotation while ensuring reliability.
- We develop **FakeInstruct**, the first million-scale dataset designed to enhance LMMs' multi-dimensional forensic capabilities in AI-generated image detection.
- We propose **FakeScope**, a multimodal expert model for transparent AI-generated image detection that integrates both detection and query-based forensic analysis. We further propose a *zero-shot* token-based strategy for estimating detection probabilities. Extensive experiments validate FakeScope's superiority in both detection and transparency-related tasks, outperforming other LMMs and binary models across diverse datasets.

## II. RELATED WORKS

Recently, the rapid advancement of image generation technology has driven growing interest in AI-generated image forensics, and the evolution of LMMs has opened new avenues for enhancing the trustworthiness of image forensic systems. We first outline the progression of AI-generated image detection techniques, followed by an overview of the current developments in LMMs.

### A. AI-generated Image Detection

The detection of AI-generated images aims to differentiate fake images (synthesized by generative AI algorithms) from real ones (created or captured by humans). This problem is commonly formulated as a binary classification task. Preexistent approaches generally incorporate forensic patterns to classify, which can be categorized into the flaw-based [18], [19] and fingerprints-based [20]–[23] according to their forensic ground. The flaw-based methods capture the intricate details in low (*e.g.*, texture [18]) or high (*e.g.*, physical rules [19], [24]) semantic levels, while the fingerprints-based detectors identify the invisible leftover patterns of generators (*e.g.*, frequency artifacts [20]–[23]). Moreover, investigations on model’s generalization ability towards unseen [3]–[6], [25], [26] and generator attribution [27], [28] have emerged. Some of them assume to be only accessible to real images and utilize generators (like an autoencoder) to simulate generative artifacts [22], [25], [26], [29]. Although remarkable, current fake image detection models still fall short in the interpretability towards human [30], which causes the detection results hard-to-explain for the general populace and weakens the credibility of model output. Therefore, developing an expert dedicated to fake image detection with both high detection accuracy and transparency is currently urgently needed.

### B. Large Multimodal Models

Typical LMMs comprise a modality encoder, a large language model (LLM), with a modality interface for cross-modal connection [31], [32]. The specialty of LMM lies in their ability to effectively receive, process, and generate multimodal information. Currently, LMMs are developing by leaps and bounds and have exhibited remarkable visual-language capabilities on par with or even surpassing the human, including the closed-source models (*e.g.*, GPT-4V [33], Gemini [34], and Claude [35]) and the open-source ones (*e.g.*, LLaVA [36], mPLUG-Owl [37], deepseek [38]). Furthermore, to adapt general-purpose LMMs to specialized fields, recent researchers proposed various expert models based on visual instruction tuning [36], [39]–[41]. Despite great progress, recent studies [7] indicate that LMMs’ forensic capabilities are still unsatisfactory, especially when it comes to identifying fine-grained forgery aspects. On the other hand, human crowd-sourcing data for visual instruction tuning becomes increasingly hard to get, partially due to the process being time-consuming, especially when multimodal information is considered. In this work, to infuse the forensic abilities on AI-generated images into foundational LMMs, we construct the

first visual instruction tuning dataset centering on fake image detection, the **FakeInstruct**, aiming at a unified multimodal paradigm based on LMMs for more transparent image forensics.

## III. FAKECHAIN: REASONING ON IMAGE AUTHENTICITY

In this section, we elaborate on the construction of **FakeChain**, a large-scale dataset with long and comprehensive *reasoning* on underlying trace evidence for authenticity. It functions as the source of forensic knowledge and further contributes to building the instruction dataset and the forensic model. For construction, we first prepare images (Sec. III-A) and then collect authenticity reasoning. While human annotation remains the most intuitive and widely applied approach for training LMMs [36], [42], acquiring sufficiently fine-grained dataset for authenticity reasoning is highly labor-intensive. To mitigate the prohibitive costs, a natural idea is to use a human-machine collaboration strategy. Therefore, we first collect human expert feedback (Sec. III-B) as weak supervision in the proposed *Anthropomorphic Chain-of-Thought Inference* (ACoTI) strategy (Sec. III-C) for forensic reasoning collection.

### A. Image Preparation

**FakeChain** contains both AI-generated and real images in equal quantities. In contrast to the one-to-all generalization setting in some works [3]–[6], [25], [26], FakeChain is deliberately constructed with a high degree of diversity to capture a broad range of generative patterns. In particular, AI-generated images function as the knowledge source of forensic trace evidence. To ensure content diversity, we sampled 23,797 AI-generated images from multiple sources. These generators span 17 types, including GAN-based, diffusion-based, autoregressive, and proprietary models. In specific, we choose representative ProGAN [43], StyleGAN [44], BigGAN [45], CogView2 [46], ADM [47], IF [48], FuseDream [49], VQDM [50], Glide [51], SD [52], SDXL [53], FLUX.1 [54], Firefly [55], Dalle2 [56], Dalle3 [57], Wukong [58] and Midjourney [59]. Also, we collect 23,797 real images from DIV2K [60], RAISE [61], and ImageNet [62]. The details of image components are provided in the supplementary material (SM).

### B. Human Expert Feedback

As shown in Fig. 3, we require a few human annotations in *step1-steer* and *step2-demonstrate* of ACoTI, including the trace evidence category and reasoning demonstration respectively. Therefore, we conduct a well-controlled *in-lab* experiment involving 30 *trained* human experts with experience in image generation as annotators, ensuring qualified understanding of generative patterns. For *step1-steer*, experts are required to correctly distinguish whether the image is AI-generated, and then select supporting categories, ensuring only accurate judgments contribute to the dataset. In practice, we provide a category set for reference  $\mathcal{F} = \{texture, edge, clarity, light\&shadow, anatomy, layout, symmetry, reflection,$

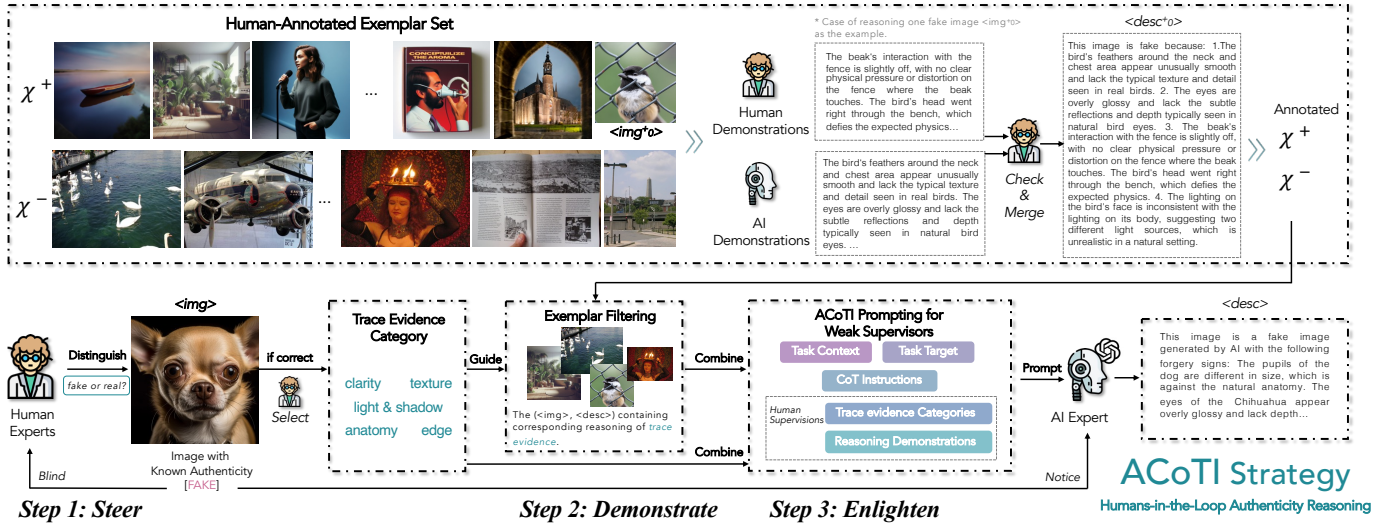


Fig. 3. Pipeline of the proposed *ACoTI* strategy for obtaining the reasoning on trace evidence under the human-machine collaboration scheme. *ACoTI* is cost-efficient that adopts the human-in-the-loop methodology to incorporate little human labor to *demonstrate*, *steer*, and *enlighten* non-perfect AI experts to generate qualified reasoning data. This semi-automatic strategy unburdens human labor, leverages LMM's abundant inner knowledge, and ensures reliability simultaneously.

*perspective, physics, shape, theme, content deficiency, distortion, unrealistic, overall hue* [7], which can characterize authenticity across different levels of trace evidence. Each image is annotated by two and only the intersection of selected categories is retained to improve reliability. Additionally, experts can provide supplementary authenticity-related information at will, such as specific area of occurrence and commonsense knowledge. For *step 2-demonstrate*, we fix 50 fake and 50 genuine images, and employ experts to annotate manually with detailed reasoning. These expert-annotated images constitute the exemplar sets  $\{\chi^+, \chi^-\}$  as illustrated in upper Fig. 3, where  $^+$  and  $^-$  denote AI-generated and genuine images respectively. To ensure balance, we manually guarantee each category of  $\mathcal{F}$  emerges in at least three exemplars. Herein, we establish the necessary human supervision for the subsequent reasoning collection.

### C. Reasoning on Visual Trace Evidence

1) *Task Definition:* **FakeChain** encapsulates forensic knowledge to enable models a fundamental understanding between visual trace evidence and authenticity. We structure it as a *materialized reasoning process*, comprising an exhaustive description of the appearance and location of trace evidence, enclosed with an authenticity conclusion. Compared with free-form descriptions, this structured reasoning format has two advantages: (1) it allows for a precise and detailed reflection of the aspects humans focus on when assessing authenticity; and (2) it inherently follows the logical pattern of human thought. For instance, when examining a suspicious image, humans first scrutinize telltale visual clues and then summarize an inclined conclusion like "Thus, I tend to think this is a fake image generated by AI". This structured reasoning approach helps LMMs more effectively mimic human decision-making in AI-

generated image detection, thereby enhancing human-centered transparency.

2) *ACoTI Strategy:* To develop a cost-efficient approach for obtaining large-scale reasoning data, we present a semi-automatic scheme to efficiently extract forensic knowledge from AI experts with few human annotations as supervision, *i.e.*, the *Anthropomorphic Chain-of-Thought Inference (ACoTI)* strategy. As illustrated in Fig. 3, *ACoTI* operates in a human-machine collaborative framework, where humans partially participate in the first and second phases by providing partial information of trace evidence. Inspired by human reasoning processes, *ACoTI* follows the *Steer-Demonstrate-Enlighten* pipeline, with the entire process detailed as follows.

**Step 1. Steer:** To utilize off-the-shelf LMMs maximally on reasoning, we employ the *category* of visual trace evidence to *steer* the reasoning process. We first notify the AI expert with the human-annotated category set  $\mathcal{F}_i$  for the  $i^{th}$  target image to ensure reasoning process focused on forensic trace evidence rather than drifting into unrelated domains. The  $\mathcal{F}_i$  directly participates in the following two steps.

**Step 2. Demonstrate:** To further mitigate hallucinations in imperfect models, we leverage human demonstrations as in-context examples, inspired by LMMs' ability to learn from explanations in context [63]. Considering the trade-off between context length and efficiency, we adaptively select the most relevant demonstrations by filtering a minimum covering set [64]  $\chi_i$  from  $\{\chi^+, \chi^-\}$  for  $\mathcal{F}_i$ . We ensure at least one positive sample and one negative sample are included in  $\chi_i$  via optimizing the following process:

$$\chi_i = \arg \min_{\chi' \subseteq \{\chi^+ \cup \chi^-\}} |\chi'|, \quad (1)$$

$$s.t. \quad L(\chi') = \mathcal{F}_i, \quad \chi' \cap \chi^+ \neq \emptyset, \quad \chi' \cap \chi^- \neq \emptyset,$$

where  $L(\cdot)$  represents the mapping function that extracts the categories covered by a given subset of exemplars. This

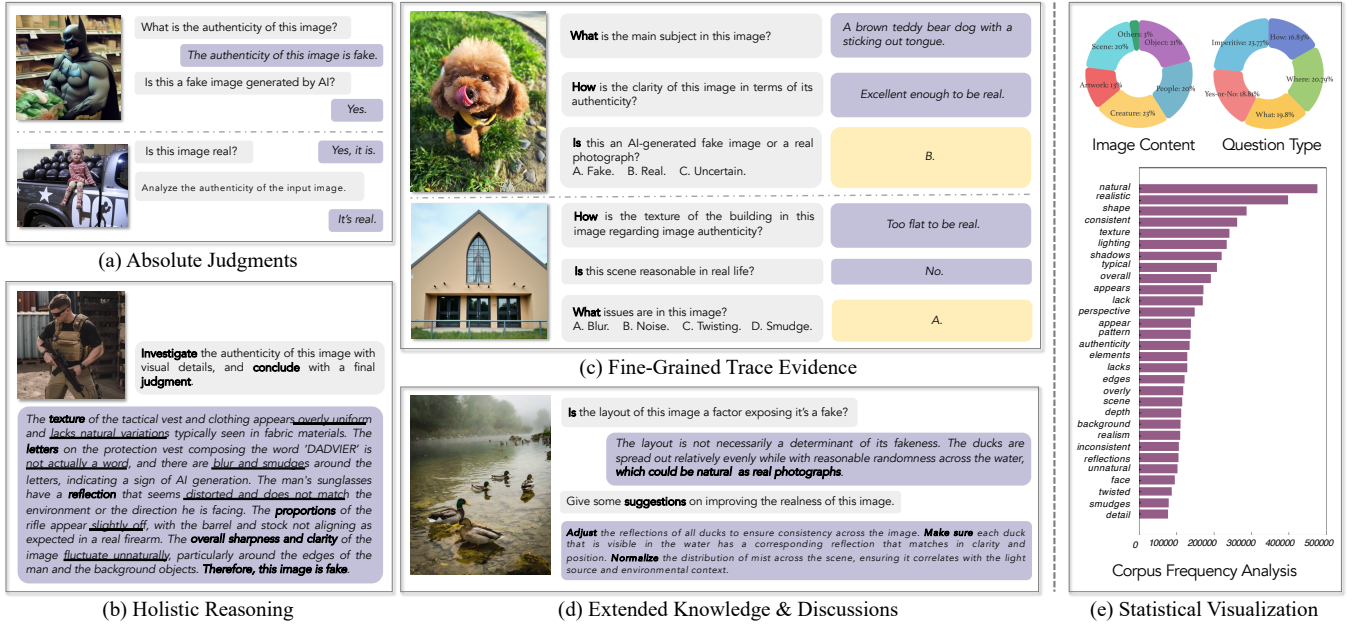


Fig. 4. The composition of the **FakeInstruct** which is derived from the FakeChain dataset, containing 47K visual instructions on absolute authenticity judgments, 95K instructions on holistic reasoning, 715K on fine-grained visual trace evidence, and 1190K on extended knowledge and discussions. The million-scale diversified visual instructions of FakeInstruct enable LMMs with both broad and fine-grained understanding of image authenticity, ensuring LMMs are equipped to handle diverse forensic tasks with both interpretability and accuracy.

ensures the selected examples can comprehensively represent the key forensic attributes required for reasoning.

**Step 3. Enlighten:** The core of ACoTI lies in enlightening the AI expert through a carefully structured prompting scheme. As illustrated in Fig. 3, the proposed ACoTI prompting emulates human reasoning process with few-shot chain-of-thought (CoT) prompting [65]. A unique aspect is explicitly providing the AI with the correct authenticity label in the context, guiding the model toward the appropriate answer space [65]. Finally, this framework is structured as a quadruple:  $\langle context, target, human supervisions, CoT prompt \rangle$ , where human supervision contains  $\mathcal{F}_i$ ,  $\chi_i$  and  $auth_i$ . Detailed prompts are provided in the SM.

In this way, ACoTI provides an effective pipeline for distilling forensic knowledge from strong models into usable reasoning data. Compared with manually collecting long and complex descriptions from human annotators, ACoTI significantly reduces the burden while maintaining data quality. To quantify its effectiveness, we further conducted a two-alternative forced choice (2AFC) study on human preference between the outcomes generated with ACoTI and those without. Six annotators rated on 100 randomly sampled annotated images, and ACoTI demonstrated 99.17% preference, indicating its effectiveness as a cost-efficient approach for extracting forensic knowledge from imperfect models. Therefore, we apply ACoTI to all collected images and organize the resulting data into the predefined *reasoning* format *rsn*. As shown in Fig. 4(b), we provide an image with corresponding *rsn*. The 47,594 tuples of  $\{\mathbf{I}, auth, rsn\}$  compose the **FakeChain** dataset, where  $\mathbf{I}$  and *auth* denote the image and authenticity label respectively.

#### IV. FAKEINSTRUCT: MILLION-SCALE MULTIMODAL FORENSIC INSTRUCTION DATASET

Although **FakeChain** offers corpus-rich reasoning with abundant forensic knowledge, we transform it into a diverse set of visual instructions to better leverage the information embedded in long-form text. As illustrated in Fig. 2(b), we further derive instruction-following data from FakeChain in the visual question answering (VQA) format with both Mistral [66] and GPT-4o [33] in an intermingling manner to enhance linguistic and instructional diversity. We take extra precautions to remove textual contamination allowing models to infer answers without visual information, thereby ensuring the integrity of instruction-based reasoning [67]. As depicted in Fig. 4, the dataset contains 2000K diversified instructions in total, which endows LMMs with flexibility and knowledge in handling extensive forensic scenarios. The details are elaborated as follows.

**Part 1. Absolute Authenticity Judgments:** As shown in Fig. 4(a), we design diverse question formulations on absolute image authenticity to explicitly implant the concepts of *fake* and *real* in LMMs. Throughout this part, we utilize the term *fake* to denote the AI-generated images, while *real* for the opposite. While incorporating synonyms such as genuine, fault, and artificial can enhance interaction flexibility with human users, we prioritize a higher level of certainty in objective authenticity assessment in this subset.

**Part 2. Holistic Reasoning:** As shown in Fig. 4(b), the holistic reasoning imitates human inference on image authenticity, which can foster LMMs' awareness of the relationships between multi-level visual trace evidence and the overall authenticity. Additionally, the carefully structured cause-and-effect reasoning framework enhances LMMs' ability to distin-

guish AI-generated images by activating their latent reasoning capabilities [68].

**Part 3. Fine-grained Trace Evidence:** To equip LMMs with the ability to seamlessly respond to diverse forensic queries from users, we decompose and reformat the reasoning data in FakeChain into a variety of visual instructions, structured in narrative or multiple-choice question (MCQ) [69] formats. This transformation is facilitated by GPT-4o [33] and Mistral [66], whose complementary strengths ensure a diverse distribution of instructional corpus. As illustrated in Fig. 4(c), the dataset includes authenticity-related VQAs covering *what*, *how*, *yes-or-no*, and *imperative* question types. These questions pertain to perceptual adjectives (e.g., unnatural, misaligned), questionable visual attributes (e.g., smudge, shape), regions of occurrence (e.g., right eye, apple skin), or contextual knowledge (e.g., shadow in wrong directions). The MCQs comprise one correct answer alongside multiple plausible yet misleading distractors, thereby enhancing models’ ability to discern subtle visual cues while mitigating misconceptions.

**Part 4. Extensional Knowledge:** Beyond fundamental trace evidence reasoning and forensic analysis, we further incorporate extensional knowledge through open-ended discussions (Fig. 4(d)). Specifically, these discussions cover four major aspects: origins of perceptual misjudgments arising from trace evidence, suggesting improvements to enhance the realism of generation, inferring potential generator characteristics based on forensic evidence, and exploring additional user-driven inquiries related to authenticity.

We herein present a brief analysis of the FakeInstruct dataset. In total, about **2000K** visual instructions are included in the FakeInstruct dataset. As shown in Fig. 4(e), quantitatively, the image content type and instruction type are well-balanced. Qualitatively, Fig. 4(c) shows decent diversity and information consistency across instructions.

## V. FAKESCOPE: LARGE MULTIMODAL FORENSIC MODEL

In this section, we introduce the proposed large multimodal expert model, **FakeScope**, which leverages state-of-the-art LMMs as its backbone and is further fine-tuned on **FakeInstruct** to incorporate forensic knowledge. Moreover, we propose a non-trivial probability estimation strategy via token soft-scoring, which could extend the model’s *qualitative* authenticity judgments to *quantifiable* probability estimations, without requiring additional explicit training on numerical labels. The details are elaborated as follows.

### A. Architecture and Supervised Instruction Tuning

The architecture of **FakeScope** follows the LLaVA-style [36] vision-language model (VLM) framework, comprising an image encoder that transforms images into tokenized representations, an LLM for textual interpretation and generation, and a vision-language connector that bridge modalities. As listed in Table I, to validate the universality of FakeInstruct, we incorporate two different model architectures, including the 7B scale LLaVA-v1.5 [36] and mPLUG-Owl2 [37], corresponding to two variants of FakeScope. LMM training typically involves two phases: the cross-modal

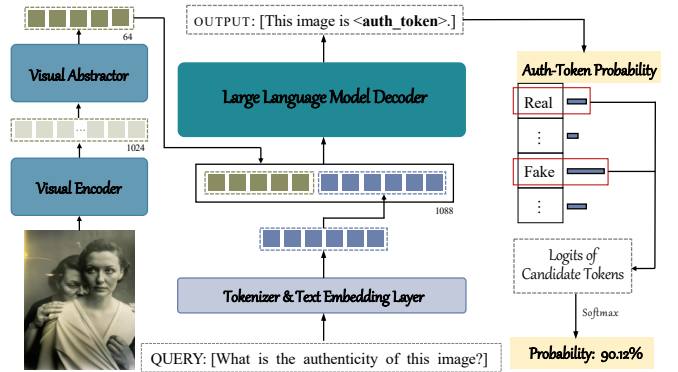


Fig. 5. Probability estimation in FakeScope. The log probabilities of candidate tokens at the `<auth_token>` position are extracted and normalized using softmax weighting to compute the predicted authenticity probability. The illustration is based on the mPLUG-Owl2 [37] backbone.

TABLE I  
META STRUCTURES OF LMMs AS FAKESCOPE FOUNDATION.

Model	Visual Model	V→L Alignment	Language Model
LLaVA-v1.5 (7B) [36]	CLIP-ViT-L14	MLP	Vicuna-7B
mPLUG-Owl2 [37]	CLIP-ViT-L14	Abstractor	LLaMA2-7B

alignment requiring gigantic-scale data and visual instruction tuning on data of proprietary domain [36]. Given the extensive scale of FakeInstruct, we introduce an auxiliary training stage to perform supervised visual instruction tuning specifically on **FakeInstruct**. Verified by previous studies [70], adequate tuning on the visual instructions in FakeInstruct is expected to facilitate the model’s visual forensic capabilities while also preserving the general knowledge obtained from earlier-phase training. To optimize efficiency, we freeze the vision encoder and fine-tune only the modality projector and language model.

### B. Probability Estimation via Token Soft-Scoring

LMMs typically convey their forensic judgment through *hard* token selection, *i.e.*, choosing the token with the highest logit when generating responses. Here, “token” refers to the vocabulary-level prediction unit in the model’s output distribution, with each token associated with a logit indicating its selection likelihood. This approach inherently limits their ability to provide **numerical probability scores**, which are crucial for assessing model confidence. Moreover, general-purpose LMMs are not explicitly trained as classifiers with numerical labels, making direct probability estimation an unpreferred methodology. To address this limitation, FakeScope is trained using binary authenticity judgments and incorporates a token *soft-scoring* strategy to convert model outputs into quantitative probability estimates. In specific, as depicted in Fig. 5, we define *fake* and *real* as anchor tokens and apply softmax normalization over their corresponding logits within a standardized prompting framework:

USER: <Image> What is the authenticity of this image?  
ASSISTANT: This image is [auth\_token].

TABLE II  
PUBLICLY AVAILABLE DATASETS USED FOR EVALUATION. THE ‡ NOTION INDICATES THE UNCONTAMINATED CONTENT OF THE DATASET, AND # DENOTES THE UNIT NUMBER.

Purpose	Datasets	Modality	# Real/ # Fake	Real Image Source	# Generators	Evaluation Criteria
Multimodal Forensic Capability	FakeBench [7]	Multiple	3k / 3k	ImageNet, DIV2K, COCO	10	Detecting, Interpreting, Reasoning, Fine-grained Analyzing
Generalization Capability	AntiFakePrompt‡ [71]	Single	42k / 6k	COCO	11	Detecting
	AIGCDetectBenchmark‡ [72]		74.3k / 74.3k	COCO, LSUN, FFHQ, CelebA	7	
In-the-wild Performance	WildRF [73]	Single	1.25k / 1.25k	Reddit, FB, X	Unknown	Detecting
	SynthWildX [4]		500 / 1.5k	X	3	

To compute probabilities, we extract the logits at the specific position of `[auth_token]`, denoted by  $\mathcal{T} = \{\tilde{t}_j|_{j=0}\} = \{\tilde{t}_{fake}, \tilde{t}_{real}\}$ , where  $\tilde{t}(\cdot)$  represents case variations of the anchor tokens to enhance robustness. The probability  $p_i$  of each class is then calculated as follows,

$$p_j = \frac{e^{\sum_{v \in \tilde{t}_j} z^{(v)}}}{\sum_{j=0}^1 e^{\sum_{v \in \tilde{t}_j} z^{(v)}}}, \quad (2)$$

where  $z^{(v)}$  represents the logit associated with token  $v$ . By leveraging token-level probability distributions rather than solely selecting the most probable token, this approach retains nuanced confidence signals that would otherwise be discarded during deterministic text generation. This enables FakeScope to generate **quantifiable probability estimates**, improving its interpretability as a forensic detector.

## VI. EXPERIMENTS AND ANALYSES

### A. Protocols

In this section, we present a systematic evaluation of FakeScope, analyzing several key aspects of its performance:

- **Multimodal Forensic Capabilities:** We evaluate to what extent the FakeScope can function as a *transparent* image forensic model (Sec. VI-B).
- **In-the-wild Performance:** We assess FakeScope’s performance on user-generated images collected from social networks (Sec. VI-C).
- **Generalization Capability:** We examine how well FakeScope generalizes to unseen image content and generators (Sec. VI-D).

Additionally, we perform ablation studies to analyze the impact of different training data components and scales (Sec. VI-E). Detailed experimental setups are provided below.

1) *Implementation Details:* Training FakeScope is implemented with PyTorch on eight Nvidia H20-NVLink 98G GPUs, and the evaluations are conducted on one NVIDIA Tesla A100 40G GPU. All training are set to full-schedule mode, with detailed parameter configurations provided in SM. To ensure FakeScope serves as a unified forensic model for AI-generated images, we retain a single checkpoint per base model for all evaluations, ensuring fair comparisons. Furthermore, to prevent data leakage, no images from the testing datasets are reused in the training data. To ensure fairness, no data augmentation strategy is employed throughout the entire training process of FakeScope.

2) *Evaluation Datasets:* We evaluate the proposed FakeScope’s multifaceted performance on five commonly used datasets in the area of AI-generated image detection. As listed in Table II, we validate multimodal forensic capabilities on FakeBench [7], covering both binary authenticity and multimodal forensic criteria. To assess generalization to *unseen* content and generation models, we use Antifake-Prompt [71], which contains fake images derived from real Microsoft COCO [74] images that are unseen during training. Additionally, we employ the non-overlapping subset of AIGCDetectBenchmark [72], excluding samples overlapping with ImageNet [62] to avoid contamination and ensure fair generalization evaluation. We further test FakeScope on user-generated images from social networks to support in-the-wild evaluation, using the WildRF [73] and SynthWildX [4] datasets, where authenticity labels are derived from social tags. It is worth noting that the scenarios like deepfakes (*e.g.* the FF++ dataset [75]) and are treated as out-of-distribution (OOD) cases, given their fundamental difference from fully AI-generated images. Nonetheless, they are included in our generalization evaluation to assess the model’s adaptability.

3) *Baseline Models:* The proposed FakeScope is compared with a diverse set of models, including open-sourced LMMs (InstructBLIP [76], IDEFICS-Instruct [77], InternLM-XComposer2-vl [31], LLaVA-v1.5 [36], Qwen-VL [78], mPLUG-Owl2 [37]), proprietary LMMs (GPT-4V [33], GeminiPro [34], Claude3-Sonnet [35]), data-driven binary forensic models (CNNSpot [20], UnivFD [3], FreDect [22]), and the vision-language contrastive model CLIP-ViT-Large-14 [79]. For detection evaluation, LMMs supports both *qualitative* (textual judgments) and *quantitative* (probabilistic estimation) settings, whereas binary detectors are limited to the *quantitative* mode. To ensure fair comparisons, the data-driven models are retrained on the same images as FakeScope without data augmentation, and all tested LMMs are evaluated using same prompting templates as FakeScope. These settings remain consistent across all experiments unless explicitly stated otherwise.

4) *Performance Measures:* FakeScope is versatile in coping with forensic detection and in-depth analysis simultaneously. To comprehensively evaluate its multidimensional capabilities, we adopt a range of metrics. For forensic detection, we consider both *qualitative* and *quantitative* settings. Specifically, *qualitative* classification accuracy is measured by  $Acc = N_c / N_t$ , where  $N_c$  and  $N_t$  denote the number of correct and total predictions, respectively. For *quantitative*

TABLE III

FORENSIC DETECTION RESULTS ON THE FAKEBENCH-FAKECLASS [7] DATASET UNDER THE *qualitative* SETTING. THE DETECTION ACC (%) OF EACH MODEL IS REPORTED. THE FIRST AND SECOND BEST LMMs ARE HIGHLIGHTED IN **BOLD** AND UNDERLINED, RESPECTIVELY. THE “FAKE” COLUMN REPORTS THE AVERAGE ACCURACY ACROSS ALL INDIVIDUAL “GENERATION MODEL” COLUMNS, AND BOTH THE AVERAGED “AUTHENTICITY” COLUMNS AND “QUESTION TYPE” COLUMNS REFLECT THE “OVERALL” COLUMN.

Subcategories	Authenticity				Question Type										Overall
	Fake	Real	What	Yes/No	proGAN	styleGAN	CogView	FuseDream	VQDM	Glide	SD	DALL-E2	DALL-E3	MJ	
Random guess	42.27	58.03	51.80	48.50	40.33	36.00	51.67	33.67	38.00	44.67	32.33	47.67	37.67	60.67	50.15
Human (Best)	97.00	93.00	/	/	100.00	100.00	100.00	100.00	100.00	100.00	100.00	100.00	100.00	93.00	87.50
Human (Worst)	43.00	13.00	/	/	50.00	0.00	46.15	77.78	33.33	16.67	41.67	7.14	14.29	0.00	55.00
Human (Overall)	76.91	72.12	/	/	95.47	58.82	87.07	95.90	63.96	82.91	79.41	77.66	70.69	45.59	74.51
GPT-4V (Proprietary, teacher)	59.87	96.20	76.33	79.73	95.00	66.00	66.67	81.33	36.67	49.00	45.67	44.33	61.00	53.00	78.03
GeminiPro (Proprietary)	35.83	99.27	61.27	73.83	45.33	15.67	47.33	52.67	19.33	28.00	35.33	35.67	41.00	38.00	67.50
Claude3 Sonnet (Proprietary)	12.00	98.23	55.97	54.27	7.00	0.00	20.33	13.67	0.67	2.67	15.33	9.33	30.33	20.67	55.12
InternLM-XC.2-v1 (InternLM2-7B)	32.17	92.33	60.40	64.10	54.00	12.67	43.33	49.00	19.00	20.33	29.33	29.67	34.67	29.67	62.25
InstructBLIP (Vicuna-7B)	67.80	47.67	65.23	50.23	80.67	65.33	66.00	71.33	68.00	70.33	60.33	61.00	70.67	64.33	57.73
Qwen-VL (Qwen-7B)	28.57	84.27	51.17	61.17	45.67	5.67	35.00	37.67	8.33	14.33	31.33	21.00	46.67	40.00	56.42
IDEFICS-Instruct (LLaMA-7B)	24.97	31.97	7.00	49.93	19.67	27.33	24.33	28.33	27.67	24.00	23.67	23.67	24.00	27.00	28.47
LLaVA-v1.5 (Vicuna-7B, baseline)	38.67	97.93	98.67	59.63	44.33	17.33	45.33	55.33	23.00	28.33	39.67	0.00	0.00	41.00	57.70
mPLUG-Owl2 (LaMA2-7B, baseline)	49.60	93.97	71.87	71.70	56.33	10.00	72.00	75.33	19.33	32.00	56.00	55.00	64.00	56.00	71.78
<b>FakeScope (Ours, mPLUG-Owl2)</b>	<b>99.50</b>	<b>99.87</b>	<b>99.73</b>	<b>99.63</b>	<b>100.00</b>	<b>100.00</b>	<b>99.67</b>	<b>100.00</b>	<b>100.00</b>	<b>100.00</b>	<u>98.67</u>	<b>100.00</b>	<u>97.67</u>	<b>99.00</b>	<b>99.68</b>
Improvement	+49.90	+5.90	+27.86	+27.93	+43.67	+90.00	+27.67	+24.67	+80.67	+68.00	+42.67	+45.00	+33.67	+43.00	+27.90
<b>FakeScope (Ours, LLaVA-v1.5)</b>	<b>98.67</b>	<b>97.93</b>	<b>98.67</b>	<b>99.63</b>	<b>99.67</b>	<b>98.67</b>	<b>99.00</b>	<b>99.67</b>	<b>96.67</b>	<b>97.00</b>	<b>99.33</b>	<b>100.00</b>	<b>98.00</b>	<b>98.67</b>	<b>98.30</b>
Improvement	+60.67	+20.53	+42.90	+38.30	+55.34	+81.34	+53.67	+44.34	+73.67	+68.67	+59.66	+100.00	+98.00	+57.67	+40.60

assessment, we follow [3], [20] and use threshold-independent calibration metrics, including average precision (AP) and area under the receiver operating characteristic curve (AUC), which are robust to class imbalance across datasets. To assess transparency-related performance, we evaluate the alignment between model responses and reference answers by employing both conventional word-level metrics (*i.e.*, BLEU [80], ROUGE [81], and BERTScore [82]) and the LLM-as-a-judge strategy [83] to measure semantic-level alignment, following [7], [16], [36], [40]. The measures are then normalized and averaged to obtain the overall reflection, where higher values indicate better performance on transparency-related abilities. Details on evaluation measures are provided in SM.

### B. Multimodal Forensic Capability

The multimodal forensic capabilities of the proposed **FakeScope** model are quantitatively assessed on FakeBench containing FakeClass, FakeClue, and FakeQA subsets with respect to four ability criteria for LMMs comprehensively defined in [7], which are stated as follows.

- **Detecting**, which evaluates whether forensic classifiers can accurately differentiate AI-generated fake images from real ones;
- **Interpreting**, which examines how well LMMs can extract visual evidence to support the *known* authenticity;
- **Reasoning**, which assesses whether LMMs can identify generative visual trace evidence and correctly infer the *unknown* image authenticity;
- **Fine-grained Analyzing**, which investigates whether LMMs can discuss and analyze specific aspects of telltale visual clues.

In practice, all LMM responses are generated using the *greedy search* strategy to ensure reproducibility. The quantitative evaluation results for the four criteria are presented below, with qualitative examples provided in SM.

**1) Detection Task:** Simple detection of fake and real images is the fundamental capability of forensic detectors. In Table III, we compare the performance of the proposed **FakeScope** with other LMMs under the *qualitative* setting on the FakeClass dataset. The FakeClass dataset contains 6,000 diversified query-answer pairs for judging absolute image authenticity with balanced authenticity proportions and adequate query diversity. The detection accuracy is measured by the correctness of responses to these queries. As reflected in the results, FakeScope of the two versions simultaneously exhibits noticeable improvements in detection reliability across all generators, authenticity categories, and query types, suggesting that **FakeInstruct can significantly enhance the forensic awareness of LMMs on binary classification**. Notably, **FakeScope achieves a peak accuracy of 99.68%, outperforming even the best-performing human expert**, and marking a significant milestone in automated forensic analysis. In Fig. 6, we further present the performance comparison using calibration measures under the *quantitative* setting. In this case, one can still witness a consistently significant advantage across all categories over both other LMMs, indicating the effectiveness of the proposed probability estimation strategy based on token soft-scoring. Notably, since we do not explicitly incorporate numerical values as the supervision when training LMMs as forensic detectors, the results further suggest that **LMMs can effectively adapt to hard authenticity labels via the internalized probabilistic reasoning process and perform well on estimating numerical probabilities**. In particular, despite being trained with the same image data, CNNSpot [20], UnivFD [3], and FreDect [22] exhibit inferior performance compared with FakeScope. While these data-driven methods can be effective in some scenarios, their performance often benefits from elaborate data augmentation [20]. In contrast, under the controlled setting of this study where no image-level augmentation is applied, purely training with binary labels



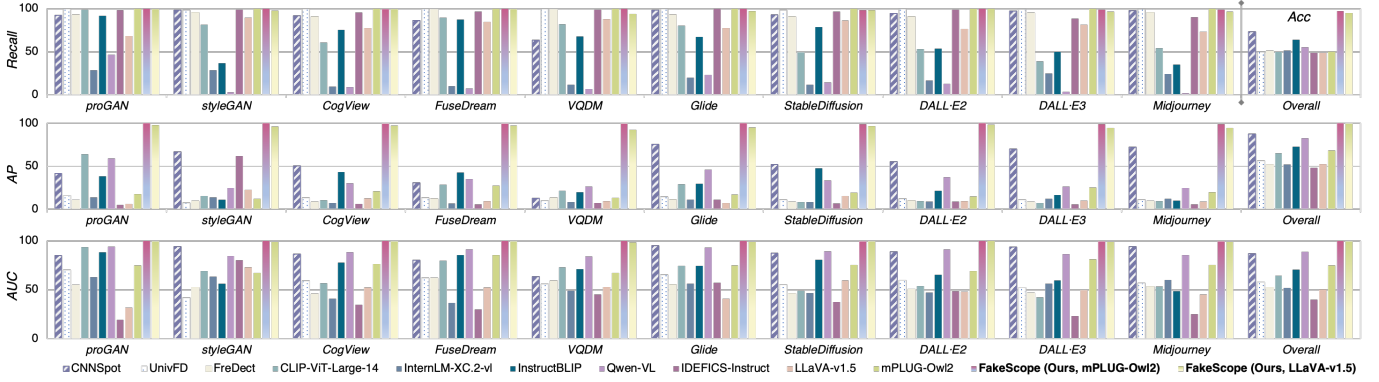


Fig. 6. Forensic detection results on FakeClass [7] under the *quantitative* setting. Calibration measures Acc (threshold is set to 0.5 for balanced indication), AP, and AUC (%) are reported for each model. The **FakeScope** far exceeds the other models on each subset and the entire dataset.

TABLE IV

MULTIMODAL FORENSIC CAPABILITY COMPARISONS ON FAKEBENCH [7], INCLUDING DETECTING ON FAKECLASS, INTERPRETING ON FAKECLUE-FAULTFINDING, REASONING ON FAKECLUE-INFERENCING, AND FINE-GRAINED FORGERY ANALYZING ON FAKEQA. THE B.-1/B.-2 DENOTE BLEU-1/2, R.-L IS ROUGE-L, SIM. IS BERTSCORE SIMILARITY, AND  $\alpha$ ,  $\rho$ ,  $\kappa$  CORRESPOND TO *completeness*, *preciseness*, AND *relevance* JUDGED BY LLMs. THE FIRST- AND SECOND-BEST PERFORMANCES OF EACH COLUMN ARE HIGHLIGHTED IN **BOLD** AND UNDERLINED, RESPECTIVELY.

Capabilities	Interpreting								Reasoning								Fine-grained Analyzing								Overall			
	Word-level				Semantic-level				Avr.↑	Word-level				Semantic-level				Avr.↑	Word-level				Semantic-level				Avr.↑	
	B.-1	B.-2	R.-L	Sim.	$\alpha$	$\rho$	$\kappa$	B.-1		B.-2	R.-L	Sim.	$\alpha$	$\rho$	$\kappa$	B.-1	B.-2		R.-L	Sim.	$\alpha$	$\rho$	$\kappa$					
GPT-4V (Teacher)	0.188	0.092	0.211	0.635	1.872	1.423	<u>1.891</u>	0.573	0.273	0.118	0.225	0.612	1.392	0.777	1.503	0.460	0.062	0.022	0.177	0.455	1.518	1.261	1.869	0.477	0.503			
GeminiPro	0.068	0.029	0.113	0.459	1.688	1.024	1.271	0.415	0.168	0.059	0.181	0.485	0.833	0.561	1.239	0.331	0.178	0.071	0.199	0.365	1.247	0.675	1.686	0.402	0.383			
Claude3 Sonnet	0.130	0.042	0.170	0.467	1.516	1.182	1.884	0.483	0.188	0.062	0.193	0.528	0.928	0.441	1.456	0.357	0.038	0.012	0.158	0.398	1.254	1.091	1.886	0.429	0.423			
InstructBLIP	0.207	0.072	0.206	0.463	1.841	1.398	1.829	0.541	0.166	0.065	0.160	0.458	1.828	0.922	1.546	0.464	0.004	0.001	0.007	0.079	0.810	0.321	0.543	0.151	0.385			
IDEFICS-Instruct	0.093	0.032	0.140	0.367	<b>1.936</b>	1.344	1.789	0.501	0.099	0.026	0.148	0.457	1.178	0.450	0.967	0.308	0.189	0.086	0.231	0.381	1.165	0.456	1.483	0.370	0.393			
InternLM-XC.2-vl	0.095	0.032	0.142	0.402	<u>1.899</u>	1.260	1.534	0.475	0.108	0.032	0.169	0.492	1.004	0.670	1.167	0.337	0.146	0.054	0.173	0.366	1.208	0.719	1.623	0.388	0.400			
LLaVA-v1.5	0.143	0.047	0.159	0.466	1.812	0.964	1.621	0.468	0.151	0.051	0.167	0.465	0.905	0.404	1.166	0.311	0.128	0.051	0.161	0.360	1.259	0.757	1.659	0.394	0.391			
Qwen-VL	0.056	0.018	0.096	0.322	1.853	1.149	1.485	0.432	0.130	0.045	0.159	0.469	0.929	0.401	1.104	0.303	0.076	0.026	0.105	0.241	1.004	0.490	0.802	0.247	0.327			
mPLUG-Owl2	0.099	0.032	0.146	0.455	1.721	0.839	1.415	0.423	0.109	0.034	0.160	0.458	0.843	0.500	1.070	0.296	0.187	0.091	0.228	0.439	1.089	0.412	1.504	0.368	0.362			
<b>FakeScope-M</b>	<b>0.434</b>	<b>0.256</b>	<b>0.371</b>	0.704	1.897	<u>1.608</u>	<b>1.901</b>	<u>0.638</u>	<b>0.439</b>	<b>0.264</b>	<b>0.383</b>	<b>0.747</b>	<b>1.886</b>	<b>1.265</b>	<u>1.775</u>	<b>0.614</b>	0.290	0.174	0.293	0.603	<u>1.628</u>	<u>1.356</u>	<u>1.857</u>	<u>0.540</u>	0.597			
Improvement	<u>+0.335</u>	<u>+0.224</u>	<u>+0.225</u>	<u>+0.249</u>	<u>+0.176</u>	<u>+0.769</u>	<u>+0.486</u>	<u>+0.215</u>	<u>+0.330</u>	<u>+0.230</u>	<u>+0.223</u>	<u>+0.289</u>	<u>+1.043</u>	<u>+0.765</u>	<u>+0.705</u>	<u>+0.318</u>	<u>+0.103</u>	<u>+0.083</u>	<u>+0.065</u>	<u>+0.164</u>	<u>+0.539</u>	<u>+0.944</u>	<u>+0.353</u>	<u>+0.172</u>	<u>+0.235</u>			
<b>FakeScope-L</b>	<u>0.432</u>	0.254	0.370	<b>0.708</b>	1.893	<b>1.653</b>	1.887	<b>0.640</b>	<u>0.437</u>	<u>0.262</u>	<u>0.381</u>	0.745	<u>1.873</u>	<u>1.242</u>	<b>1.776</b>	0.610	<b>0.304</b>	<b>0.184</b>	<b>0.305</b>	<b>0.611</b>	<b>1.647</b>	<b>1.402</b>	<b>1.879</b>	<b>0.553</b>	<b>0.601</b>			
Improvement	<u>+0.289</u>	<u>+0.207</u>	<u>+0.211</u>	<u>+0.242</u>	<u>+0.081</u>	<u>+0.689</u>	<u>+0.266</u>	<u>+0.172</u>	<u>+0.286</u>	<u>+0.211</u>	<u>+0.214</u>	<u>+0.280</u>	<u>+0.968</u>	<u>+0.838</u>	<u>+0.610</u>	<u>+0.299</u>	<u>+0.176</u>	<u>+0.133</u>	<u>+0.144</u>	<u>+0.251</u>	<u>+0.388</u>	<u>+0.645</u>	<u>+0.220</u>	<u>+0.159</u>	<u>+0.210</u>			

may fall short in capturing the intricacies of forensic cues. This further underscores the effectiveness of the multimodal information in FakeInstruct and highlights LLMs’ superiority to integrate multimodal information for AI-generated image forensics.

2) *Interpreting Task*: We find out that incorporating visual trace evidence into training can significantly enhance the interpretation ability of LLMs. In practice, LLMs are evaluated using the *fault-finding* prompting mode of FakeClue, where models are instructed to explain image authenticity based on visual clues, such as in the prompt “This is a fake image generated by AI, explain the reasons”. In the first category of Table IV, the two variants of FakeScope demonstrate substantial improvements in interpreting ability, especially the word-level similarities and semantic relevance level to the ground truth. These findings indicate that training on FakeInstruct conspicuously enhances the *effect-to-cause* awareness concerning the forensic attributes of LLMs.

3) *Reasoning Task*: Forensic reasoning is the inverse of interpretation, assessing LLMs’ inference capability in deriving authenticity judgments from visual trace evidence. This

task is evaluated using the prompts in the *inference* mode of FakeClue, such as “Inspect this image carefully and formulate an evaluation regarding its authenticity”. As observed in the experimental results listed in the second category of Table IV, while all baseline LLMs generally exhibit weak forensic reasoning capabilities, the proposed FakeScope achieves a substantial improvement after training on FakeInstruct and even surpasses all compared models, reaching SOTA performance. Most notably, its reasoning capability also outperforms the teacher model GPT-4V [33] by over 30%, demonstrating the effectiveness of FakeInstruct in enhancing *cause-to-effect* forensic awareness and triggering forensic reasoning in LLMs.

4) *Fine-Grained Analyzing Task*: To further evaluate the effectiveness of FakeScope in analyzing specific aspects of image forgery, we conduct experiments on the FakeQA dataset, which consists of queries regarding fine-grained visual forgeries. As shown in the third category of Table IV, FakeScope exhibits notable improvements over both baseline models and its teacher model, highlighting its enhanced fine-grained forensic analyzing capabilities. However, despite these

promising results, this ability still shows room for improvement compared to the other two transparency-related forensic capabilities interpreting and reasoning. This suggests potential avenues for further optimization, particularly in refining its sensitivity to subtle forgery artifacts.

### C. In-the-wild Performance

To evaluate the **real-world applicability** of our model, we conduct in-the-wild experiments on diverse, unstructured image data collected from social media, including WildRF [73] and SynthWildX [4]. These datasets contains real-world samples with various distortions, such as compression artifacts, post-processing modifications, and noise, which pose additional challenges for forensic models. The testing protocol aligns with other experiments, and all LMMs are evaluated in the quantitative setting. The AP and AUC values for detection are listed in Table V. As reflected by the results, FakeScope equipped with mPLUG-Owl2 [37] consistently outperforms other state-of-the-art methods across the majority of generators, achieving superior overall performance in the in-the-wild testing. Notably, it demonstrates competitive results on images generated by Dalle3 and Midjourney, ranking second only to CNNSpot [20]. These findings highlight FakeScope’s robustness and effectiveness in handling unconstrained image content and generation models, reinforcing its adaptability to real-world forensic challenges beyond in-lab benchmarks.

### D. Generalization Capability

For forensic detectors, the generalization ability on unacquainted image contents and generators is crucial for practical deployment. To assess this, we conduct a more challenging experiment to evaluate whether FakeScope is well generalizable on **unseen** image content and generators. Practically, we test all methods on the uncontaminated content proportions of AntifakePrompt [71] and AIGCDetectBenchmark [72], in comparison with the data employed in FakeInstruct. In particular, the AntifakePrompt dataset covers several OOD tasks beyond the primary scope of this work, such as image super-resolution, face spoofing [75], and inpainting, which pose a greater challenge to model generalization and robustness. In Table VI, the AP and AUC scores of each model across 17 image generators are presented, including 6 seen and 11 unseen ones. We also present the average AP over unseen generators as well as over all generators. From Table VI, it can be observed that the two variants of the FakeScope can achieve SOTA performance across all 17 generators and, notably, outperforms all baselines on the set of unseen generators. These results demonstrate that FakeScope can effectively handle novel image content and generation techniques, indicating strong generalization capability.

Furthermore, we analyze model stability by plotting detection accuracy as a function of the decision threshold ( $\in (0, 1)$ ) for each method, thereby assessing their sensitivity to threshold selection across different generators. In Fig. 7, a separate curve is shown for each forensic detector by averaging detecting accuracy across all generators in each dataset. Unlike AUC and mAP, the accuracy (Acc) is highly

sensitive to threshold variation, and models with unstable performance may suffer under suboptimal thresholds, leading to less robustness. It can be observed from Fig. 7 that both versions of FakeScope exhibit highly consistent peak accuracy across different datasets and maintain stable performance over a broad range of threshold values. In contrast, other models show considerable variability in optimal accuracy across datasets and are overly sensitive to specific threshold settings. This indicates that FakeScope possesses prominent robustness towards forensic threshold across different datasets and generators, thereby enhancing its applicability in real-world scenarios.

### E. Ablation Studies

To investigate the influence of different data components and scales on training FakeScope, we further conduct ablation studies on the influence of three aspects during tuning with mPLUG-Owl2 [37]: (1) scale of training data; (2) collaboration of FakeChain and visual instructions; and (3) participation of multimodal contextual information.

**1) Effects of Training Data Scale:** To effectively handle data-scarce scenarios is crucial for forensic models, yet it remains increasingly challenging due to the high cost and difficulty of acquiring high-quality training data. To evaluate the effectiveness of **FakeInstruct** dataset, we randomly sample four subsets—80%, 60%, 40%, and 20%—while preserving the original data composition, and analyze the impact on training outcomes. As illustrated in Fig. 8, the resulting FakeScope variants exhibit remarkable resilience to performance degradation as the available training data decreases, demonstrating the strong utility of FakeInstruct. Notably, the transparency-related performance remains a significant improvement over the baselines, even at the extreme 20% data proportion, and continues to strengthen as the training data size grows. This trend highlights the effectiveness of the multimodal forensic knowledge embedded in FakeInstruct, further demonstrating that the reasoning data can substantially enhance the forensic capabilities of large multimodal models.

**2) Effects of Collaborative Training:** During training, we combine different subsets to jointly optimize a unified forensic foundation model. To validate the effectiveness of this strategy, we compare it against task-specific training focused solely on transparent forensic capabilities. As indicated by the results listed in Table VII, the collaborative training scheme—integrating long-form reasoning with granular visual instructions—yields significant improvements in model performance. Although the various subsets in **FakeInstruct** originate from a shared data source, this strategy remains cost-efficient and enables FakeScope to generalize more effectively across diverse forensic tasks, demonstrating greater stability across a broader knowledge domain.

**3) Effects of Multimodal Awareness:** A defining feature that sets **FakeScope** apart from conventional binary forensic detectors is its integration of rich multimodal contextual information on visual trace evidence during training. While these data are aimed at enhancing transparency-related forensic capabilities, they might affect the performance on simple

TABLE V

IN-THE-WILD FORENSIC DETECTION ABILITY ON WILD<sub>RF</sub> [73] AND SYNTH<sub>WILD</sub>X [4] CONTAINING USER-GENERATED IMAGE CONTENT AND UNKNOWN GENERATORS. THE AP AND AUC (%) ARE REPORTED, AND THE FIRST- AND SECOND-BEST PERFORMERS FOR EACH CATEGORY ARE HIGHLIGHTED IN **BOLD** AND UNDERLINE RESPECTIVELY.

Datasets	Wild <sub>RF</sub>			Synth <sub>WILD</sub> X			Average
	Reddit	FB	X	Dalle3	Firefly	MJ	mAP $\uparrow$ /AUC $\uparrow$
CNNSpot ( <i>training-based</i> )	84.20/ 82.94	79.58/ 79.27	86.62/ 86.46	<b>91.21/ 91.85</b>	83.72/ 83.39	<b>87.19/ 87.26</b>	85.42/ 85.20
UnivFD ( <i>training-based</i> )	49.83/ 48.65	55.54/ 56.35	54.89/ 53.67	41.77/ 38.22	55.21/ 56.05	45.88/ 42.83	50.52/ 49.29
FreDect ( <i>training-based</i> )	46.95/ 47.27	51.97/ 52.62	48.25/ 48.21	45.26/ 45.65	46.77/ 45.38	50.99/ 52.86	48.37/ 48.67
CLIP-ViT-Large-14 ( <i>zero-shot</i> )	45.64/ 45.52	38.93/ 34.05	44.07/ 42.94	42.33/ 38.19	42.26/ 38.56	42.37/ 37.39	42.60/ 39.44
InternLM-XC.2-v1 ( <i>InternLM2-7B</i> )	42.87/ 38.76	49.93/ 51.08	42.36/ 38.97	50.06/ 52.65	56.39/ 59.33	48.39/ 49.68	48.67/ 48.41
InstructBLIP ( <i>Vicuna-7B</i> )	53.75/ 54.82	40.54/ 34.92	45.65/ 42.31	41.24/ 36.38	42.24/ 38.63	49.56/ 48.13	45.83/ 42.53
Qwen-VL ( <i>Qwen-7B</i> )	40.85/ 37.65	36.46/ 26.29	35.16/ 22.67	36.44/ 27.06	39.15/ 32.64	34.85/ 20.34	36.48/ 27.11
IDEFICS-Instruct ( <i>LLaMA-7B</i> )	46.69/ 45.90	45.96/ 43.65	41.24/ 34.70	37.41/ 27.92	39.93/ 33.36	40.29/ 32.50	41.92/ 36.69
LLaVA-v1.5 ( <i>Vicuna-7B, baseline</i> )	58.79/ 62.41	51.66/ 49.45	50.67/ 51.70	53.30/ 56.43	49.03/ 49.68	54.70/ 56.45	53.36/ 54.78
mPLUG-Owl2 ( <i>LLaMA-7B, baseline</i> )	58.52/ 59.66	51.96/ 50.30	47.72/ 45.29	48.23/ 48.05	46.34/ 48.33	47.67/ 46.16	51.74/ 49.63
<b>FakeScope (Ours, mPLUG-Owl2)</b>	<b>91.89/ 91.45</b>	<b>85.31/ 85.43</b>	<b>92.96/ 92.14</b>	89.02/ 89.43	<b>88.04/ 88.56</b>	83.72/ 84.04	<b>88.49/ 88.51</b>
<b>FakeScope (Ours, LLaVA-v1.5)</b>	80.01/ 78.60	67.94/ 73.23	75.48/ 76.09	87.37/ 87.44	78.94/ 81.76	81.99/ 83.40	78.46/ 80.09

TABLE VI

GENERALIZATION CAPABILITY VALIDATED ON ANTIFAKE<sub>PROMPT</sub> [71] AND AIGC<sub>DETECT</sub>BENCHMARK [72]. THE AP (%) OF VARIOUS CLASSIFIERS ACROSS 17 INDIVIDUAL GENERATORS ARE REPORTED. CHANCE IS 50% AND BEST POSSIBLE PERFORMANCE IS 100%. ALL THE LMMs ARE TESTED UNDER THE *quantitative* SETTING. VALUES IN GRAY REPRESENT THE GENERATORS SEEN IN TRAINING. NO CONTENT OVERLAPPING EXISTS IN THE RESULTS. THE BEST MODEL IN EACH COLUMN IS HIGHLIGHTED IN **BOLD**.

Datasets	AIGCDetectBenchmark							AntifakePrompt							Unseen	Average			
	Pro	Style	Star	Gau	Style2	WFIR	Control	SD2	SDXL	IF	Dalle2	SGXL	LaMa	SD2Inpaint			LTE	SD2SR	DeepFake
CNNSpot	64.86	61.41	70.33	60.10	63.08	56.41	70.19	82.85	92.51	86.50	56.61	60.25	48.88	52.15	50.54	50.22	95.15	60.71	66.00
UnivFD	61.37	50.36	39.78	55.61	48.49	51.91	56.22	43.25	35.75	44.24	45.36	58.17	50.85	57.46	80.99	60.68	68.42	57.24	53.47
FreDect	49.93	55.13	49.99	53.26	54.93	49.97	53.61	29.79	37.78	38.36	35.80	44.46	49.86	49.93	48.02	49.81	56.10	50.63	47.45
CLIP-ViT-Large-14	89.22	71.12	94.92	88.58	64.40	81.17	60.43	29.20	31.87	37.28	49.44	70.85	62.86	63.26	85.15	71.71	41.85	71.38	64.31
InternLM-XC.2-v1	52.15	46.40	61.16	50.47	52.28	44.29	68.72	35.73	41.03	48.59	45.49	62.15	52.39	58.33	60.58	58.46	71.70	58.23	53.52
InstructBLIP	50.27	40.79	32.31	88.63	40.42	49.36	55.46	25.98	29.87	25.86	72.11	64.04	59.18	74.46	95.64	81.84	97.48	67.17	57.86
Qwen-VL	72.27	42.91	41.39	82.54	44.80	48.92	84.18	75.39	69.55	72.97	83.83	88.15	66.50	78.31	93.55	89.05	91.31	73.52	72.10
IDEFICS-Instruct	40.26	51.87	53.68	39.40	47.26	66.99	35.16	22.03	23.55	25.85	22.45	41.24	46.53	41.11	34.81	44.27	48.49	45.36	40.29
mPLUG-Owl2	58.44	48.91	83.24	51.39	45.26	41.84	69.79	45.10	46.10	44.71	55.03	74.34	50.71	57.82	77.64	68.28	71.16	62.86	58.22
LLaVA-v1.5	40.97	44.09	41.30	38.08	43.03	56.01	42.36	24.32	25.07	26.71	32.78	45.13	47.93	45.08	37.69	43.91	80.87	47.40	42.08
<b>FakeScope (mPLUG-Owl2)</b>	89.70	92.96	88.63	89.83	86.94	93.32	98.20	97.27	99.17	98.80	99.04	<b>99.77</b>	<b>98.20</b>	<b>98.99</b>	<b>99.72</b>	<b>98.80</b>	<b>99.96</b>	<b>95.67</b>	95.84
<b>FakeScope (LLaVA-v1.5)</b>	99.92	98.01	<b>100.00</b>	<b>99.66</b>	<b>98.01</b>	<b>99.45</b>	<b>98.96</b>	98.21	99.04	99.10	99.04	99.65	82.59	95.97	96.40	97.20	73.64	94.68	<b>96.17</b>

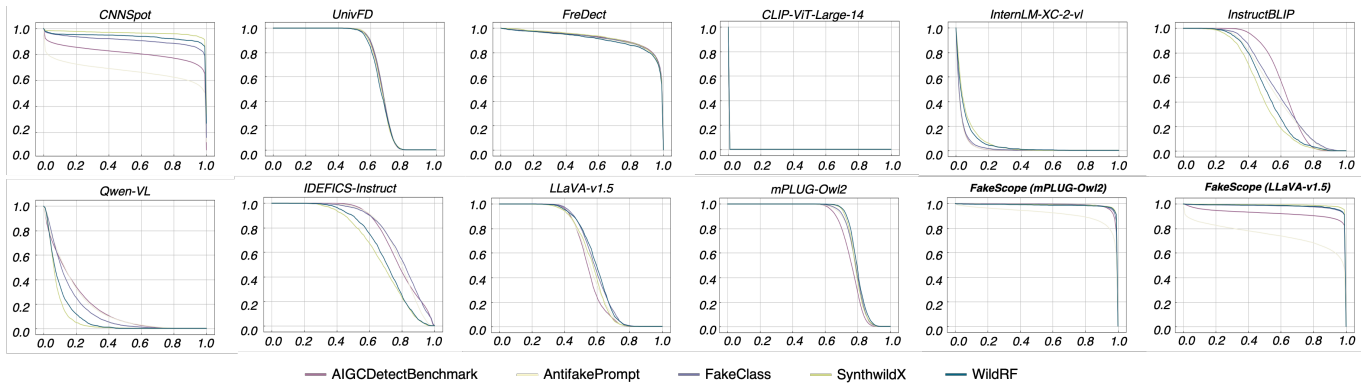


Fig. 7. Accuracy as a function of detection threshold. For each model, we present the relations between the detection threshold (x-axis) and accuracy (y-axis) on all generators of five testing databases. It turns out the FakeScope of two versions of base models (the last two sub-figures) is the only one that can achieve a great bargain between threshold sensitivity and detection accuracy, indicating remarkable robustness.

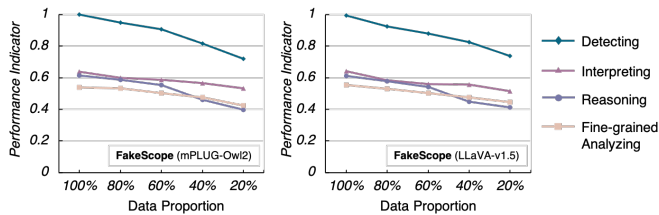


Fig. 8. Performance on FakeBench [7] with respect to training data scale, demonstrating the effectiveness of FakeInstruct data. The x-axis indicates the proportion of FakeInstruct used for training and the y-axis is the corresponding performance indicator of each ability dimension.

TABLE VII

COMPARISON ON TRANSPARENT FORENSIC CAPABILITIES BETWEEN *only* FAKECHAIN AND *full* FAKEINSTRUCT AS TRAINING DATASET. THE BEST PERFORMANCE OF EACH COLUMN IS HIGHLIGHTED IN **BOLD**.

Training Strategy	Detect	Interpret	Reason	Analyze
none ( <i>baseline</i> )	58.22%	0.423	0.296	0.368
<i>only</i> FakeChain	83.27%	0.593	0.576	0.350
<i>full</i> FakeInstruct	<b>99.68%</b>	<b>0.638</b>	<b>0.614</b>	<b>0.540</b>

TABLE VIII

COMPARISON ON FORENSIC DETECTION ABILITY BETWEEN *full* FAKEINSTRUCT, *only* ABSOLUTE JUDGMENT, AND *only* CONTEXTUAL DATA. THE AP (%) ON EACH DATASET IS REPORTED. THE BEST PERFORMANCE OF EACH COLUMN IS HIGHLIGHTED IN **BOLD**.

Dataset/ Training Strategy	none ( <i>baseline</i> )	<i>only</i> absolute	<i>only</i> contextual	<i>full</i> ( <i>employed</i> )
FakeBench [7]	68.37	94.06 <sub>+25.96</sub>	84.13 <sub>+15.76</sub>	<b>99.94</b> <sub>+31.57</sub>
AntiFakePrompt [71]	60.06	90.12 <sub>+30.06</sub>	74.84 <sub>+14.78</sub>	<b>98.90</b> <sub>+38.84</sub>
AIGCDetectBenchmark [72]	54.84	81.65 <sub>+26.81</sub>	60.73 <sub>+5.89</sub>	<b>90.23</b> <sub>+35.39</sub>
WildRF [73]	52.73	82.34 <sub>+29.61</sub>	62.54 <sub>+9.81</sub>	<b>90.05</b> <sub>+37.32</sub>
SynthWildX [4]	47.41	82.78 <sub>+35.37</sub>	52.59 <sub>+5.18</sub>	<b>86.93</b> <sub>+39.52</sub>

detection. To validate whether such information also improves pure forensic detection, we compare the performance of models trained with and without it. As compared in Table VIII, incorporating contextual information not only improves the model’s transparency but also enhances detection accuracy and generalization, even when using the same amount of image data. In contrast, omitting absolute authenticity labels from training results in inconsistent improvements. These findings suggest that multimodal forensic cues can strengthen the model’s task awareness and fine-grained visual comprehension, enabling it to more effectively attend to forensic-relevant patterns. However, the model’s detection performance still heavily relies on absolute authenticity judgments, as relying solely on descriptive cues may introduce ambiguity into the decision-making process for authenticity.

## VII. CONCLUSIONS AND FUTURE WORK

In this paper, we propose a multimodal paradigm for transparent AI-generated image forensics, versatile in detection, in-depth analysis, and extended discussions. Based on the advanced cross-modal capability of large multimodal models (LMMs), we collect and leverage rich image forensic knowledge to enhance their forensic awareness. By emulating human

causal inference based on visual trace evidence, we introduce a human-machine collaborative strategy and construct the first large-scale dataset containing structured forensic reasoning data. This reasoning foundation is further expanded into a million-scale visual instruction dataset, which is internalized into LMMs to improve their transparent forensic abilities on AI-generated images. Extensive experiments demonstrate consistent effectiveness of this paradigm across LMMs with varied meta frameworks. The proposed expert forensic model can reliably handle multiple forensic tasks under a unified paradigm, and exhibits strong generalization and in-the-wild capabilities. Besides, we discovered that LMMs can effectively align with hard authenticity labels and demonstrate impressive generalization on estimating numerical probabilities, even without explicit supervision.

This work not only presents a viable pathway toward transparent AI-generated image forensics, but also offers insights into the development of trustworthy AI risk management within the broader multimodal landscape. Moreover, the proposed model could serve as the source of generating cross-modal forensic information, which may further support the development of more reliable forensic systems. Notwithstanding the use of advanced models such as GPT-4V to distill forensic knowledge, it may still represent an early-stage effort in the evolving trajectory of large multimodal models. While some uncertainties remain, this study nonetheless demonstrates the effectiveness of multimodal information and the feasibility of forensic transparency. We intend to further explore the abilities of newly emerged LMMs and contribute model update to community. Looking ahead, future efforts may focus on enhancing the model’s few-shot adaptability and dialectical reasoning capability for better robustness and explanatory power in more complex forensic contexts.

## REFERENCES

- [1] S. Yan, O. Li, J. Cai, Y. Hao, X. Jiang, Y. Hu, and W. Xie, “A sanity check for ai-generated image detection,” *arXiv preprint arXiv:2406.19435*, 2024.
- [2] Y. Zou, P. Li, Z. Li, H. Huang, X. Cui, X. Liu, C. Zhang, and R. He, “Survey on ai-generated media detection: From non-mlm to mlm,” *arXiv preprint arXiv:2502.05240*, 2025.
- [3] U. Ojha, Y. Li, and Y. J. Lee, “Towards universal fake image detectors that generalize across generative models,” in *IEEE Int. Conf. Computer Vision and Pattern Recognition*, 2023, pp. 24 480–24 489.
- [4] D. Cozzolino, G. Poggi, R. Corvi, M. Nießner, and L. Verdoliva, “Raising the bar of ai-generated image detection with clip,” in *IEEE Int. Conf. Computer Vision and Pattern Recognition*, 2024, pp. 4356–4366.
- [5] D. Cozzolino, G. Poggi, M. Nießner, and L. Verdoliva, “Zero-shot detection of AI-generated images,” in *European Conf. on Computer Vision*, 2024.
- [6] J. Ricker, D. Lukovnikov, and A. Fischer, “Aeroblade: Training-free detection of latent diffusion images using autoencoder reconstruction error,” in *IEEE Int. Conf. Computer Vision and Pattern Recognition*, 2024, pp. 9130–9140.
- [7] Y. Li, X. Liu, X. Wang, B. S. Lee, S. Wang, A. Rocha, and W. Lin, “Fakebench: Probing explainable fake image detection via large multimodal models,” *arXiv preprint arXiv:2404.13306*, 2024.
- [8] Y. Zhang, B. Colman, A. Shahriyari, and G. Bharaj, “Common sense reasoning for deep fake detection,” *European Conf. on Computer Vision*, 2024.
- [9] K. Sun, S. Chen, T. Yao, H. Yang, X. Sun, S. Ding, and R. Ji, “Towards general visual-linguistic face forgery detection,” *arXiv preprint arXiv:2307.16545*, 2023.

- [10] J. Ye, B. Zhou, Z. Huang, J. Zhang, T. Bai, H. Kang, J. He, H. Lin, Z. Wang, T. Wu *et al.*, “Loki: A comprehensive synthetic data detection benchmark using large multimodal models,” *Int. Conf. on Learning Representations*, 2025.
- [11] Z. Xu, X. Zhang, R. Li, Z. Tang, Q. Huang, and J. Zhang, “Fakeshield: Explainable image forgery detection and localization via multi-modal large language models,” *Int. Conf. on Learning Representations*, 2025.
- [12] J. Liu, F. Zhang, J. Zhu, E. Sun, Q. Zhang, and Z.-J. Zha, “Forgerypt: Multimodal large language model for explainable image forgery detection and localization,” *arXiv preprint arXiv:2410.10238*, 2024.
- [13] Z. Huang, J. Hu, X. Li, Y. He, X. Zhao, B. Peng, B. Wu, X. Huang, and G. Cheng, “Sida: Social media image deepfake detection, localization and explanation with large multimodal model,” *arXiv preprint arXiv:2412.04292*, 2024.
- [14] Z. Huang, B. Xia, Z. Lin, Z. Mou, W. Yang, and J. Jia, “Ffaa: Multimodal large language model based explainable open-world face forgery analysis assistant,” *arXiv preprint arXiv:2408.10072*, 2024.
- [15] Y. Chen, Z. Yan, S. Lyu, and B. Wu, “X-DFD: A framework for explainable and extendable deepfake detection,” 2025. [Online]. Available: <https://openreview.net/forum?id=EoTIIDT0Tr>
- [16] S. Wen, J. Ye, P. Feng, H. Kang, Z. Wen, Y. Chen, J. Wu, W. Wu, C. He, and W. Li, “Spot the fake: Large multimodal model-based synthetic image detection with artifact explanation,” *arXiv preprint arXiv:2503.14905*, 2025.
- [17] Y. Zhang, A. Unell, X. Wang, D. Ghosh, Y. Su, L. Schmidt, and S. Yeung-Levy, “Why are visually-grounded language models bad at image classification?” *Advances in Neural Information Processing Systems*, 2024.
- [18] N. Zhong, Y. Xu, Z. Qian, and X. Zhang, “Rich and poor texture contrast: A simple yet effective approach for ai-generated image detection,” *arXiv preprint arXiv:2311.12397*, 2023.
- [19] U. A. Ciftci, I. Demir, and L. Yin, “Fakecatcher: Detection of synthetic portrait videos using biological signals,” *IEEE Trans. Pattern Analysis and Machine Intelligence*, 2020.
- [20] S.-Y. Wang, O. Wang, R. Zhang, A. Owens, and A. A. Efros, “CNN-generated images are surprisingly easy to spot... for now,” in *IEEE Int. Conf. Computer Vision and Pattern Recognition*, 2020, pp. 8695–8704.
- [21] R. Durall, M. Keuper, and J. Keuper, “Watch your up-convolution: CNN based generative deep neural networks are failing to reproduce spectral distributions,” in *IEEE Int. Conf. Computer Vision and Pattern Recognition*, 2020, pp. 7890–7899.
- [22] J. Frank, T. Eisenhofer, L. Schönherr, A. Fischer, D. Kolossa, and T. Holz, “Leveraging frequency analysis for deep fake image recognition,” in *International conference on machine learning*. PMLR, 2020, pp. 3247–3258.
- [23] M. Wolter, F. Blanke, R. Heese, and J. Garcke, “Wavelet-packets for deepfake image analysis and detection,” *Machine Learning*, vol. 111, no. 11, pp. 4295–4327, 2022.
- [24] A. Sarkar, H. Mai, A. Mahapatra, S. Lazebnik, D. A. Forsyth, and A. Bhattad, “Shadows don’t lie and lines can’t bend! generative models don’t know projective geometry... for now,” in *IEEE Int. Conf. Computer Vision and Pattern Recognition*, 2024, pp. 28 140–28 149.
- [25] B. Liu, F. Yang, X. Bi, B. Xiao, W. Li, and X. Gao, “Detecting generated images by real images,” in *European Conference on Computer Vision*. Springer, 2022, pp. 95–110.
- [26] Y. Jeong, D. Kim, Y. Ro, P. Kim, and J. Choi, “Fingerprintnet: Synthesized fingerprints for generated image detection,” in *European Conference on Computer Vision*. Springer, 2022, pp. 76–94.
- [27] Z. Sha, Z. Li, N. Yu, and Y. Zhang, “De-fake: Detection and attribution of fake images generated by text-to-image generation models,” in *Proceedings of the 2023 ACM SIGSAC Conference on Computer and Communications Security*, 2023, pp. 3418–3432.
- [28] Z. Wang, C. Chen, Y. Zeng, L. Lyu, and S. Ma, “Where did i come from? origin attribution of ai-generated images,” *Advances in neural information processing systems*, vol. 36, 2024.
- [29] X. Zhang, S. Karaman, and S.-F. Chang, “Detecting and simulating artifacts in gan fake images,” in *IEEE international workshop on information forensics and security*, 2019, pp. 1–6.
- [30] L. Lin, N. Gupta, Y. Zhang, H. Ren, C.-H. Liu, F. Ding, X. Wang, X. Li, L. Verdoliva, and S. Hu, “Detecting multimedia generated by large ai models: A survey,” *arXiv preprint arXiv:2402.00045*, 2024.
- [31] X. Dong, P. Zhang, Y. Zang, Y. Cao, B. Wang, L. Ouyang, X. Wei, S. Zhang, H. Duan, M. Cao *et al.*, “Internlm-xcomposer2: Mastering free-form text-image composition and comprehension in vision-language large model,” *arXiv preprint arXiv:2401.16420*, 2024.
- [32] Y. Huang, Q. Yuan, X. Sheng, Z. Yang, H. Wu, P. Chen, Y. Yang, L. Li, and W. Lin, “AesBench: An expert benchmark for multimodal large language models on image aesthetics perception,” *arXiv preprint arXiv:2401.08276*, 2024.
- [33] OpenAI, “GPT-4 technical report,” *CoRR*, vol. abs/2303.08774, 2023.
- [34] G. Team, R. Anil, S. Borgeaud, Y. Wu, J.-B. Alayrac, J. Yu, R. Soricut, J. Schalkwyk, A. M. Dai, A. Hauth *et al.*, “Gemini: a family of highly capable multimodal models,” *arXiv preprint arXiv:2312.11805*, 2023.
- [35] Anthropic, “Introducing the next generation of claude,” <https://www.anthropic.com/news/claude-3-family>, 2024.03.
- [36] H. Liu, C. Li, Q. Wu, and Y. J. Lee, “Visual instruction tuning,” *Advances in Neural Information Processing Systems*, vol. 36, 2024.
- [37] Q. Ye, H. Xu, J. Ye, M. Yan, A. Hu, H. Liu, Q. Qian, J. Zhang, and F. Huang, “mplug-owl2: Revolutionizing multi-modal large language model with modality collaboration,” in *IEEE Int. Conf. Computer Vision and Pattern Recognition*, 2024, pp. 13 040–13 051.
- [38] H. Lu, W. Liu, B. Zhang, B. Wang, K. Dong, B. Liu, J. Sun, T. Ren, Z. Li, H. Yang *et al.*, “Deepseek-v1: towards real-world vision-language understanding,” *arXiv preprint arXiv:2403.05525*, 2024.
- [39] Y. Liu, H. Duan, Y. Zhang, B. Li, S. Zhang, W. Zhao, Y. Yuan, J. Wang, C. He, Z. Liu, K. Chen, and D. Lin, “MMBench: Is your multi-modal model an all-around player?” *European Conf. on Computer Vision*, 2024.
- [40] P. Lu, S. Mishra, T. Xia, L. Qiu, K.-W. Chang, S.-C. Zhu, O. Tafjord, P. Clark, and A. Kalyan, “Learn to explain: Multimodal reasoning via thought chains for science question answering,” *Advances in Neural Information Processing Systems*, vol. 35, pp. 2507–2521, 2022.
- [41] Y. Du, H. Guo, K. Zhou, W. X. Zhao, J. Wang, C. Wang, M. Cai, R. Song, and J.-R. Wen, “What makes for good visual instructions? synthesizing complex visual reasoning instructions for visual instruction tuning,” *arXiv preprint arXiv:2311.01487*, 2023.
- [42] H. Wu, Z. Zhang, E. Zhang, C. Chen, L. Liao, A. Wang, K. Xu, C. Li, J. Hou, G. Zhai *et al.*, “Q-instruct: Improving low-level visual abilities for multi-modality foundation models,” *IEEE Int. Conf. Computer Vision and Pattern Recognition*, 2024.
- [43] T. Karras, T. Aila, S. Laine, and J. Lehtinen, “Progressive growing of GANs for improved quality, stability, and variation,” *Int. Conf. on Learning Representations*, 2018.
- [44] T. Karras, S. Laine, and T. Aila, “A style-based generator architecture for generative adversarial networks,” in *IEEE Int. Conf. Computer Vision and Pattern Recognition*, 2019, pp. 4401–4410.
- [45] A. Brock, J. Donahue, and K. Simonyan, “Large scale gan training for high fidelity natural image synthesis,” *Int. Conf. on Learning Representations*, 2019.
- [46] M. Ding, W. Zheng, W. Hong, and J. Tang, “Cogview2: Faster and better text-to-image generation via hierarchical transformers,” in *Advances in Neural Information Processing Systems*, 2022, pp. 16 890–16 902.
- [47] P. Dhariwal and A. Nichol, “Diffusion models beat gans on image synthesis,” *Advances in neural information processing systems*, vol. 34, pp. 8780–8794, 2021.
- [48] Deepfloyd, “If,” <https://github.com/deep-floyd/IF>, 2024.06.
- [49] X. Liu, C. Gong, L. Wu, S. Zhang, H. Su, and Q. Liu, “FuseDream: Training-free text-to-image generation with improved CLIP+GAN space optimization,” *arXiv preprint arXiv:2112.01573*, 2021.
- [50] S. Gu, D. Chen, J. Bao, F. Wen, B. Zhang, D. Chen, L. Yuan, and B. Guo, “Vector quantized diffusion model for text-to-image synthesis,” in *IEEE Int. Conf. Computer Vision and Pattern Recognition*. IEEE, 2022, pp. 10 696–10 706.
- [51] A. Nichol, P. Dhariwal, A. Ramesh, P. Shyam, P. Mishkin, B. McGrew, I. Sutskever, and M. Chen, “Glide: Towards photorealistic image generation and editing with text-guided diffusion models,” in *Int. Conf. on Machine Learning*, 2022, pp. 16 784–16 804.
- [52] R. Rombach, A. Blattmann, D. Lorenz, P. Esser, and B. Ommer, “High-resolution image synthesis with latent diffusion models,” in *IEEE Int. Conf. Computer Vision and Pattern Recognition*, 2022, pp. 10 684–10 695.
- [53] D. Podell, Z. English, K. Lacey, A. Blattmann, T. Dockhorn, J. Müller, J. Penna, and R. Rombach, “SDXL: improving latent diffusion models for high-resolution image synthesis,” in *Int. Conf. on Learning Representations*, 2024.
- [54] “Flux.1,” 2024. [Online]. Available: <https://blackforestlabs.ai/#get-flux>
- [55] Adobe, “Firefly,” <https://firefly.adobe.com/>, 2024.06.
- [56] A. Ramesh, P. Dhariwal, A. Nichol, C. Chu, and M. Chen, “Hierarchical text-conditional image generation with CLIP latents,” *arXiv preprint arXiv:2204.06125*, 2022.
- [57] Z. Shi, X. Zhou, X. Qiu, and X. Zhu, “Improving image captioning with better use of captions,” *Annual Meeting of the Association for Computational Linguistics*, 2020.
- [58] Wukong, “Wukong,” <https://xihe.mindspore.cn/modelzoo/wukong>, 2024.03.

- [59] Midjourney, “Midjourney,” <https://mid-journey.ai/>, 2024.06.
- [60] E. Agustsson and R. Timofte, “Ntire 2017 challenge on single image super-resolution: Dataset and study,” in *IEEE Int. Conf. Computer Vision and Pattern Recognition Workshop*, 2017, pp. 126–135.
- [61] D.-T. Dang-Nguyen, C. Pasquini, V. Conotter, and G. Boato, “Raise: A raw images dataset for digital image forensics,” in *Proceedings of ACM Multimedia Systems Conf.*, 2015, pp. 219–224.
- [62] J. Deng, W. Dong, R. Socher, L.-J. Li, K. Li, and L. Fei-Fei, “Imagenet: A large-scale hierarchical image database,” in *IEEE Int. Conf. Computer Vision and Pattern Recognition*, 2009, pp. 248–255.
- [63] A. Lampinen, I. Dasgupta, S. Chan, K. Mathewson, M. Tessler, A. Creswell, J. McClelland, J. Wang, and F. Hill, “Can language models learn from explanations in context?” in *Findings of the Association for Computational Linguistics at EMNLP 2022*, Y. Goldberg, Z. Kozareva, and Y. Zhang, Eds., Dec. 2022, pp. 537–563.
- [64] E. Balas and M. W. Padberg, “On the set-covering problem,” *Operations Research*, vol. 20, no. 6, pp. 1152–1161, 1972.
- [65] J. Wei, X. Wang, D. Schuurmans, M. Bosma, b. ichter, F. Xia, E. Chi, Q. V. Le, and D. Zhou, “Chain-of-thought prompting elicits reasoning in large language models,” in *Advances in Neural Information Processing Systems*, 2022, pp. 24 824–24 837.
- [66] A. Q. Jiang, A. Sablayrolles, A. Mensch, C. Bamford, D. S. Chaplot, D. d. l. Casas, F. Bressand, G. Lengyel, G. Lample, L. Saulnier *et al.*, “Mistral 7b,” *arXiv preprint arXiv:2310.06825*, 2023.
- [67] X. Fu, Y. Hu, B. Li, Y. Feng, H. Wang, X. Lin, D. Roth, N. A. Smith, W.-C. Ma, and R. Krishna, “Blink: Multimodal large language models can see but not perceive,” in *European Conf. on Computer Vision*. Springer, 2025, pp. 148–166.
- [68] T. Kojima, S. S. Gu, M. Reid, Y. Matsuo, and Y. Iwasawa, “Large language models are zero-shot reasoners,” *Advances in Neural Information Processing Systems*, vol. 35, pp. 22 199–22 213, 2022.
- [69] D. Schwenk, A. Khandelwal, C. Clark, K. Marino, and R. Mottaghi, “A-okvqa: A benchmark for visual question answering using world knowledge,” in *European Conf. on Computer Vision*. Springer, 2022, pp. 146–162.
- [70] K. Kumar, T. Ashraf, O. Thawakar, R. M. Anwer, H. Cholakkal, M. Shah, M.-H. Yang, P. H. Torr, S. Khan, and F. S. Khan, “Llm post-training: A deep dive into reasoning large language models,” *arXiv preprint arXiv:2502.21321*, 2025.
- [71] Y.-M. Chang, C. Yeh, W.-C. Chiu, and N. Yu, “Antifakeprompt: Prompt-tuned vision-language models are fake image detectors,” *arXiv preprint arXiv:2310.17419*, 2023.
- [72] N. Zhong, Y. Xu, S. Li, Z. Qian, and X. Zhang, “Patchcraft: Exploring texture patch for efficient ai-generated image detection,” *arXiv preprint arXiv:2311.12397*, pp. 1–18, 2024.
- [73] B. Cavia, E. Horwitz, T. Reiss, and Y. Hoshen, “Real-time deepfake detection in the real-world,” *arXiv preprint arXiv:2406.09398*, 2024.
- [74] T.-Y. Lin, M. Maire, S. Belongie, J. Hays, P. Perona, D. Ramanan, P. Dollár, and C. L. Zitnick, “Microsoft coco: Common objects in context,” in *European Conf. on Computer Vision*. Springer, 2014, pp. 740–755.
- [75] A. Rössler, D. Cozzolino, L. Verdoliva, C. Riess, J. Thies, and M. Nießner, “FaceForensics++: Learning to detect manipulated facial images,” in *IEEE Int. Conf. on Computer Vision*, 2019.
- [76] W. Dai, J. Li, D. Li, A. M. H. Tiong, J. Zhao, W. Wang, B. Li, P. Fung, and S. Hoi, “InstructBLIP: Towards general-purpose vision-language models with instruction tuning,” in *Advances in Neural Information Processing Systems*, 2023.
- [77] H. Laurençon, L. Saulnier, L. Tronchon, S. Bekman, A. Singh, A. Lozhkov, T. Wang, S. Karamcheti, A. Rush, D. Kiela *et al.*, “Obelics: An open web-scale filtered dataset of interleaved image-text documents,” *Advances in Neural Information Processing Systems*, vol. 36, pp. 71 683–71 702, 2023.
- [78] J. Bai, S. Bai, S. Yang, S. Wang, S. Tan, P. Wang, J. Lin, C. Zhou, and J. Zhou, “Qwen-vl: A versatile vision-language model for understanding, localization, text reading, and beyond,” *arXiv preprint arXiv:2308.12966*, 2023.
- [79] A. Radford, J. W. Kim, C. Hallacy, A. Ramesh, G. Goh, S. Agarwal, G. Sastry, A. Askell, P. Mishkin, J. Clark *et al.*, “Learning transferable visual models from natural language supervision,” in *Int. Conf. on Machine Learning*, 2021, pp. 8748–8763.
- [80] K. Papineni, S. Roukos, T. Ward, and W.-J. Zhu, “Bleu: a method for automatic evaluation of machine translation,” in *Annual Meeting of the Association for Computational Linguistics*, 2002, pp. 311–318.
- [81] L. Chin-Yew, “Rouge: A package for automatic evaluation of summaries,” in *Proceedings of the Workshop on Text Summarization Branches Out*, 2004.
- [82] N. Reimers and I. Gurevych, “Sentence-bert: Sentence embeddings using siamese bert-networks,” in *Proceedings of the 2019 Conference on Empirical Methods in Natural Language Processing and the 9th International Joint Conference on Natural Language Processing*. ACL, 2019, pp. 3982–3992.
- [83] C.-H. Chiang and H.-y. Lee, “Can large language models be an alternative to human evaluations?” in *Annual Meeting of the Association for Computational Linguistics*. ACL, 2023, pp. 1559–1575.